THE JOURNAL OF PHYSICAL CHEMISTRY LETTERS
A JOURNAL OF THE AMERICAN CHEMICAL SOCIETY

pubs.acs.org/JPCL

Letter

How Good Is the Vibronic Hamiltonian Repetition Approach for Long-Time Nonadiabatic Molecular Dynamics?

Wei Li and Alexey V. Akimov*

Cite This: *J. Phys. Chem. Lett.* 2022, 13, 9688−9694

Read Online

ACCESS | Metrics & More | Article Recommendations | Supporting Information

ABSTRACT: Multiple applied studies of slow nonadiabatic processes in nanoscale and condensed matter systems have adopted the "repetition" approximation in which long trajectories for such simulations are obtained by concatenating shorter trajectories, directly available from ab initio calculations, many times. Here, we comprehensively assess this approximation using model Hamiltonians with parameters covering a wide range of regimes. We find that state transition time scales may strongly depend on the length of the repeated data, although the convergence is not monotonic and may be slow. The repetition approach may under- or overestimate the time scales by a factor of ≤7−8, does not directly depend on the dispersion of energy gap and nonadiabatic coupling (NAC) frequencies, but may depend on the magnitude of the NACs. We suggest that the repetition-based nonadiabatic dynamics may be inaccurate in simulations with very small NACs, where intrinsic transition times are on the order of ≥100 ps.

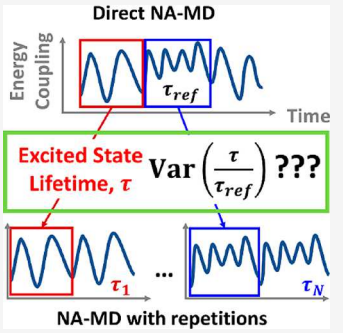

Nonadiabatic molecular dynamics (NA-MD) is a powerful technique for modeling the dynamics of excited states in various light-harvesting systems.[1] It can provide mechanistic insights into non-equilibrium charge and excitation energy transfer mechanisms and kinetics in various materials and helps in rationalizing available time-resolved spectroscopy experiments. The NA-MD simulation requires nonadiabatic couplings (NACs) and energies of electronic states that can be obtained from the on-the-fly electronic structure calculations. However, directly modeling the nonadiabatic processes that occur on time scales of hundreds of picoseconds to nanoseconds in large systems remains impossible because of the demanding computational expenses. A number of methods for extending the system size and time scales in such calculations have been developed, including the use of semiempirical wave function and tight-binding theories,[2−5] non-self-consistent approximation to hybrid functionals,[6] fragmentation-based approaches,[7−10] and machine learning (ML)-based methods.[11−20] In the latter, the short-time trajectories can be used as the training sets to create a ML model of the vibronic Hamiltonian. Once constructed, the model can be used to forecast the NACs and energy levels for indefinite times, thus providing a basis for efficient long-time NA-MD calculations, eliminating the need for expensive explicit electronic structure calculations. Similar in spirit to ML-based procedures, the quasi-stochastic Hamiltonian (QSH) NA-MD approach uses the short-time NAC and energy gap data to derive the key parameters of a new Hamiltonian that is meant to capture the essential statistical properties of the short-time data but does not aim to reproduce them exactly.[21] Prezhdo and co-workers employed inverse fast Fourier transform (iFFT) for interpolation of a vibronic Hamiltonian along a precomputed trajectory.[22] Finally, an even simpler version of this approach was utilized by several researchers. In it, the few-picosecond *ab initio* data (NACs and energies) are iterated multiple times to generate arbitrarily long time series of NACs and state energies that are subsequently used in the NA-MD calculations.[23−27] However, the validity of such a vibronic Hamiltonian repetition approach remains unexplored. It is unclear how much the time scales obtained from the repeated short-time data could vary in comparison to the reference time scales obtained from the direct simulations based on the genuine long-time data, if they would be accessible. Such an assessment would be very expensive if it were to rely solely on atomistic simulations. However, with the help of analytic model Hamiltonians, this question can be addressed.

In this work, we report our comprehensive assessment of the vibronic Hamiltonian repetition approach for NA-MD simulation. We rely on an extensive set of model Hamiltonians spanning various regions of the parameter space. We aim to address the following questions: (a) How does the overall kinetics of the state transitions depend on the lengths of the repeated data? (b) How does it depend on the intrinsic properties of the data (e.g., frequencies, their distribution, the magnitude of the energy gap and NACs, and the magnitude of their fluctuations)? We demonstrate that the results of the rNA-MD simulations depend crucially on the length of the

Received: September 7, 2022
Accepted: October 7, 2022
Published: October 11, 2022

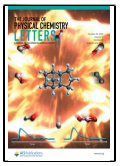

https://doi.org/10.1021/acs.jpclett.2c02765
J. Phys. Chem. Lett. 2022, 13, 9688−9694

provided data sets and the convergence toward the reference time scales is not monotonic and may not be strictly accessible. Given this result, we estimate that the variation of the time scales is generally bound to the factor of 5 for a wide range of FT frequencies and their variations. The time scale variations normally increase for slower dynamics, indicating that the repetition procedure may be less accurate for the intrinsically slower dynamics.

In our NA-MD calculations, the time-dependent wave function of an abstract system is expanded in the adiabatic basis, $\{\psi_i\}$: $\Psi(\mathbf{r}, \mathbf{R}, t) = \sum_i c_i(t)\psi_i(\mathbf{r}; \mathbf{R}(t))$, where $c_i(t)$ is the time-dependent expansion coefficients and $\mathbf{r}$ and $\mathbf{R}$ are electronic and nuclear coordinates, respectively. Here, the nuclear variables are represented by the trajectories $\mathbf{R}(t)$. Following the quantum-classical trajectory surface hopping (TSH) methodology of Tully,[28] we obtain the trajectories classically. Furthermore, we adopt the neglect of back-reaction approximation (NBRA) of Prezhdo and co-workers,[29,30] according to which the nuclear trajectories remain unaffected by the electronic state changes during the course of the NA-MD simulation. In other words, the trajectories $\mathbf{R}(t)$ are precomputed first and then used to derive the time-dependent Hamiltonians. The dynamics of electronic states is described by the time-dependent Schrodinger equations (TD-SE), $i\hbar\frac{\partial\Psi}{\partial t} = \hat{H}\Psi$. Considering the wave function ansatz presented above, it simplifies to $i\hbar\dot{c}_i(t) = H_{\text{vib}}(t)c_i(t)$. Here, $H_{\text{vib},ij}(t) = E_i(t)\delta_{ij} - i\hbar d_{ij}(t)$ is the time-dependent vibronic Hamiltonian, where $E_i(t)$ is the energy of adiabatic state i and $d_{ij}(t)$ is the scalar NAC between states i and j. Because of the NBRA, the vibronic Hamiltonian and its components are the functions of solely time. In other words, they constitute the time series. The rNA-MD approach essentially assumes that short time series already contain the essential information and therefore can be repeated indefinitely to propagate the electronic wave function (as represented by the coefficients $\{c_i(t)\}$) for as long as needed. Once the coefficients are propagated to a certain time, they can be used to compute the state hopping probabilities at that time. Because we focus on the assessment of the repetition approach, we choose to use Tully's fewest switches surface hopping (FSSH) algorithm to compute the hopping probabilities. In particular, the hopping probability between states j and k during the time interval $[t, t + \Delta t]$ is given by $g_{jk}(t, t + \Delta t) = \max[0, b_{jk}(t)\Delta t/\rho_{\text{mm}}(t)]$; $b_{jk} = -2Re[\rho_{jk}{}^*(t) d_{jk}(t)]$; $\rho_{jk}(t) = c_j(t)c_k{}^*(t)$. Following the NBRA adaptation of the TSH, the proposed hops ($j \rightarrow k$) are accepted with the probability $\exp(-\Delta E_{kj}/k_B T)$, if $\Delta E_{kj} = E_k - E_j > 0$ and 1 if $\Delta E_{kj} < 0$. Here, k_B is the Boltzmann constant and T is the temperature of the environment. The NA-MD calculations are carried out using the NBRA implementation of the FSSH method as available in the open-source Libra package[31] (version 5.2.0[32]). Further discussion of the essentials of the FSSH algorithm and its implementation within NBRA can be found elsewhere.[33]

We focus on model time-dependent Hamiltonians with energy and NAC components given as scaled and shifted superpositions of periodic functions of time (eqs 1) (details in Table S1):

$$E_i(t; a, b, c) = a\left[b + c\sum_{k=1}^{N} c_{i,k}^{\text{E}} \sin(\omega_{i,k}^{\text{E}} t)\right] \tag{1a}$$

$$d_{ij}(t; a, b, c) = a\left[b + c\sum_{k=1}^{N} c_{ij,k}^{\text{NAC}} \sin(\omega_{ij,k}^{\text{NAC}} t)\right] \tag{1b}$$

where a is the overall scaling factor used to explore different regimes of the dynamics, b is the mean value of the corresponding property before the shift, and c is the scaling that controls the fluctuation of the original unscaled ($a = 1$) data. Such a behavior is typical for many classes of systems, such as halide perovskites,[34−36] two-dimensional dichalcogenides,[37,38] monolayer black phosphorus,[39] metal particles,[40,41] colloidal semiconductor quantum dots,[42] graphene[43] and carbon nanotubes,[44−46] molecular crystals,[47] etc. The selection of the parameters b and c was motivated by the typical values of the energy gaps, the NACs, and the fluctuations of these properties in the classes of materials mentioned above. The parameter a is manually varied to accelerate or decelerate the overall dynamics. The detailed scripts implementing these model Hamiltonians can be found in the GitHub repository.[48] Our expectation is that slowing the rates of nonadiabatic transitions by using smaller NAC scaling factors could make the data repetition a cruder approximation. For instance, one could design the NAC time series with notably increased NACs at later times but smaller NACs at earlier times. If the NACs are large enough, the transitions could be completed on the ultrafast time scale, long before the trajectory would reach the region of increased NACs. Thus, the intrinsically fast transitions are expected to be less sensitive to the repetition approach. On the contrary, for smaller NAC scaling factors, the intrinsic dynamics would be slow enough to make the repetition approach yield notably different results compared to those using the genuine time series. In this situation, repeating the data without locally increased NACs present in the original time series would yield slower transitions than when using the genuine data. In this work, however, we do not consider such specially designed models explicitly. Instead, we explore a range of generic random models.

The parameters $c_{i,k}^{\text{E}}$ and $\omega_{i,k}^{\text{E}}$ correspond to the kth amplitudes and corresponding frequencies of the modes included in the time dependence of energy level i. Analogously, $c_{ij,k}^{\text{NAC}}$ and $\omega_{ij,k}^{\text{NAC}}$ are the parameters controlling the time variation of the NACs between states i and j. The form of vibronic Hamiltonian is chosen to model the typical data obtained in *ab initio* calculation of solid state and nanoscale systems within the NBRA. Such a model approach has been adopted in the earlier works of one of us, and it focused on exploring the properties of the TSH schemes within NBRA and developing new methodologies.[13,21] In the work presented here, the parameter sets $\{c_{i,k}^{\text{E}}, \omega_{i,k}^{\text{E}}\}$ and $\{c_{ij,k}^{\text{NAC}}, \omega_{ij,k}^{\text{NAC}}\}$ are chosen to represent a wide variety of electron−phonon coupling regimes as characterized by the Fourier transforms of the corresponding data and are summarized in detail in section S1 of the Supporting Information. For a simple two-state system, there are only two components of the vibronic Hamiltonian. One is the energy gap, and the other is the NAC. The fluctuation of each of them can be controlled by low-, intermediate-, or high-frequency modes or can be coupled to multiple modes spanning a wide range of frequencies.

For all parameter sets (models) considered in this work, we generate the 100 ps data series for the time-dependent vibronic Hamiltonian. We consider such data to be the reference data mimicking the direct *ab initio* calculations, as if such calculations are accessible for realistic atomistic systems. This

https://doi.org/10.1021/acs.jpclett.2c02765
J. Phys. Chem. Lett. 2022, 13, 9688−9694

mode constitutes the regular NA-MD calculation approach. We also utilize smaller subsets of such data (e.g., first 1, 5, 10, 20, or 50 ps), which are then repeated to recreate the total of 100 ps of data. This mode constitutes the rNA-MD approach. Such short data subsets represent what is typically accessible or what could be accessible in practical calculations.

Our expectations are as follows. On one hand, one can expect that the larger the repeated data unit size (fewer repetitions involved), the closer the agreement of the rNA-MD simulations to the reference data should be. Indeed, using overly short trajectories may accidentally favor the prevalence of small (case 1, Figure 1) or large (case 2, Figure 1) couplings,

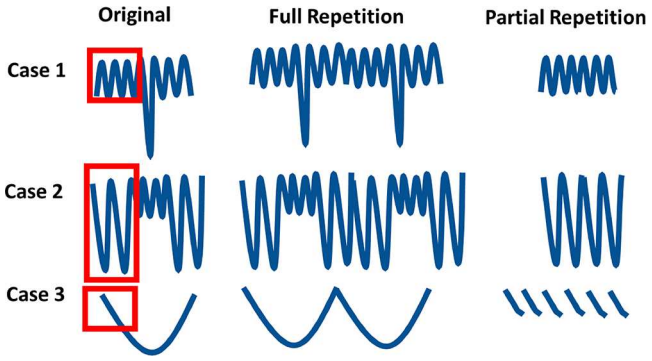

Figure 1. Schematic representation of some situations in the repetition approach.

leading to decelerating or accelerating of the corresponding transitions, respectively. Furthermore, one can expect that the repetition approximation may be better justified in situations in which the dominant vibrational modes driving the fluctuations of NACs and energy gaps are well captured by the data unit to be repeated. For instance, if the transition is coupled to a low-frequency mode, using a short data set would be inadequate, because it may not contain even a single period of the corresponding mode (e.g., case 3, Figure 1). Repeating such a short data set can significantly alter the time-dependent Hamiltonian and affect the resulting dynamics. In the example shown in case 3 in Figure 1, using an overly small repetition unit means that regions of higher NACs (for instance) would not be present in the repeated data set, and one would predict underestimated transition rates.

The comparison of the cases shown in Figure 1 also suggests that it may be easier to apply the repetition approach to the data sets with higher intrinsic frequencies, because smaller data sets would be more likely to capture the important fluctuations (e.g., compare cases 1 and 3). Indeed, in cases 1 and 3, the high-NAC regions of the time-dependent Hamiltonian are missing. However, in case 1, the larger NAC values are sampled only rarely, whereas in case 3, the larger NACs exist for longer periods of time; therefore, missing them would be more critical. On the basis of the discussions presented above, we hypothesize that the validity of the repetition approximation may be tied to the dispersion of the frequencies in the FT of the corresponding elements of the vibronic Hamiltonian. However, having dominant frequencies at 2000 and 3000 cm^{-1} is not the same as having them at 100 and 1100 cm^{-1}. Thus, it makes sense to consider the dispersion of frequencies on the logarithmic scale. We thus introduce the following parameter:

$$\sigma_X^{\,2} = \sum_i p_i'(a_i - \overline{a})^2 \tag{2a}$$

$$\overline{a} = \sum_i p_i' a_i \tag{2b}$$

$$a_i = \ln(\omega_i^X) \tag{2c}$$

$$p_i' = \frac{|p_i|}{\sum_i |p_i|} \tag{2d}$$

where X is the property in which we are interested, such as a particular NAC or energy gap, p_i' is the normalized intensity of peak i, and ω_i is the position of FT peak i. The use of the logarithmic scale in the definition of the $\sigma_X^{\,2}$ parameter also makes it invariant with respect to the choice of frequency units. To test the hypothesis presented above, we design 46 vibronic Hamiltonian models (section S1) such that they cover various regions on the ($\sigma_E^{\,2}$, $\sigma_{NAC}^{\,2}$) plane (Figure 2).

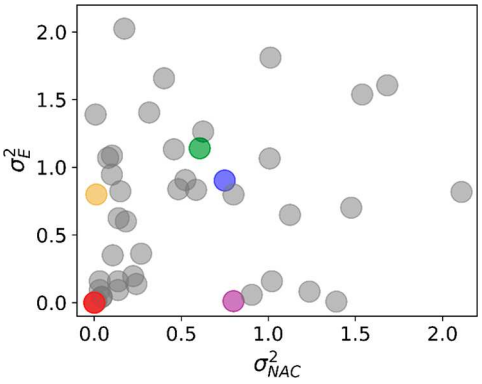

Figure 2. Representation of the 46 model Hamiltonians on the ($\sigma_E^{\,2}$, $\sigma_{NAC}^{\,2}$) plane. Model Hamiltonians 3, 5, 7, 11, and 12 discussed below correspond to red, blue, green, gold, and purple dots, respectively.

We first investigate the lifetime convergence with respect to the repeated data unit length. The lifetime variation plots for each model are summarized in Table S2. Here, we demonstrate only five representative models: models 3, 5, and 7, with 1, 20, and 40 randomly selected frequencies, respectively, in the range of 0−3000 cm^{-1}, model 11 with a high frequency of NACs and a low frequency of energy gaps, and model 12 with a low frequency of NACs and a high frequency of energy gaps (Figure 3). These models correspond to the distinctly colored dots in Figure 2. Because the mean value of the NAC magnitude in the model Hamiltonian is quite large, we consider scaling NACs by multiplying them by factors of 0.2, 0.1, and 0.05 to explore the performance of rNA-MD simulations on various time scale regimes. For the models explored (Figure 3 and section S2), we observe only a weak convergence of the computed lifetimes with respect to the size of the repeated data unit. Increasing this parameter may lead to decreasing the lifetimes (e.g., model 7), increasing them (e.g., model 5, with a scaling factor of 0.2), modest variation (e.g., model 3), or nonmonotonic behavior. A more or less monotonous convergence of the computed lifetimes with the size of the repeated data unit may be observed in some models and some scaling parameters (see section S2), but it is not guaranteed in general. This is a reasonable expectation because the repeated data unit may resemble the entirety of the data for

https://doi.org/10.1021/acs.jpclett.2c02765
J. Phys. Chem. Lett. 2022, 13, 9688−9694

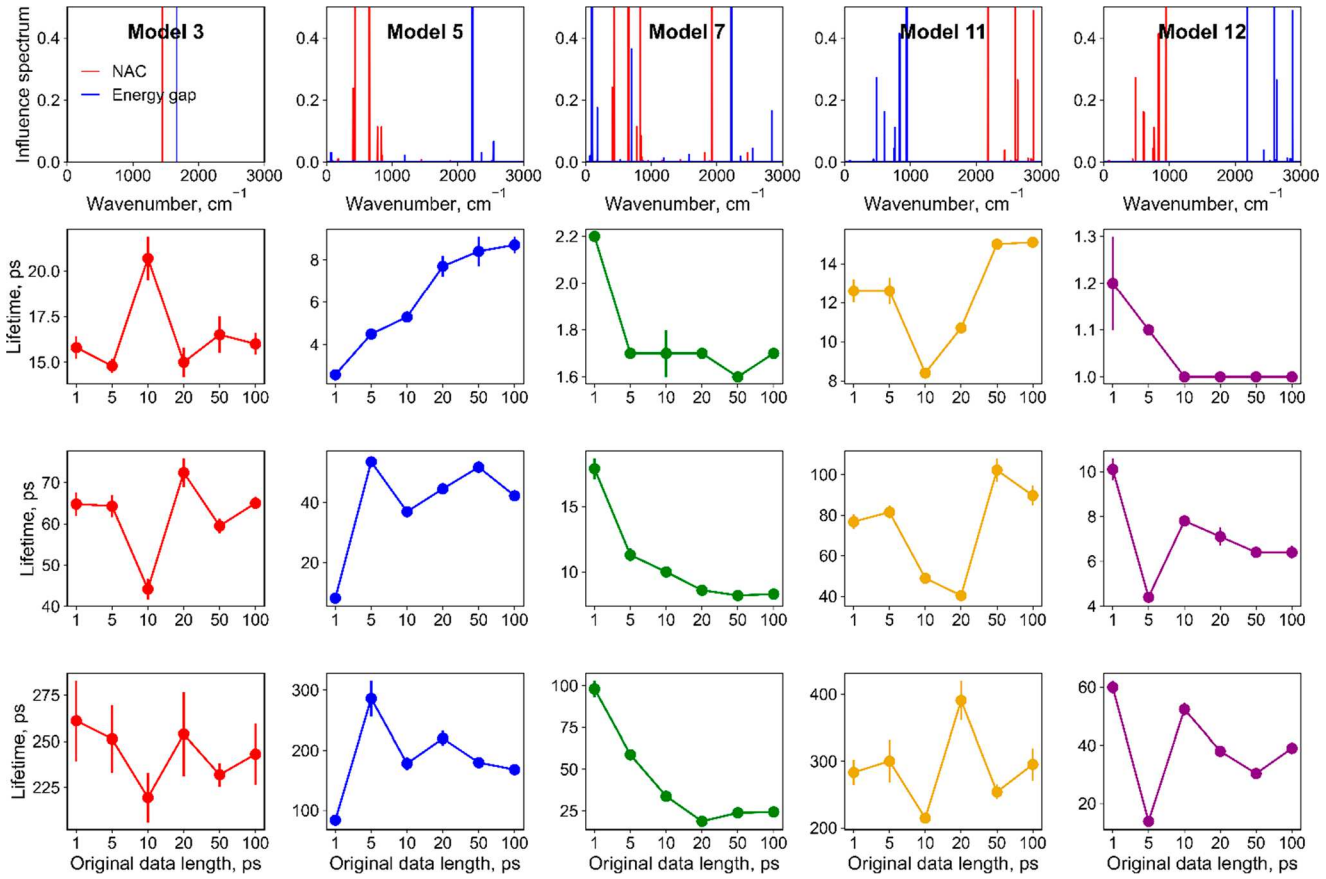

Figure 3. Influence spectrum of the energy gap and NAC (first row). Dependence of the excited state lifetime on the repeated data unit size (second to fourth rows) with NAC scaled by 0.2, 0.1, and 0.05, respectively. Each column corresponds to one of the model Hamiltonians used.

a hypothetical infinitely long trajectory. Thus, it is more appropriate to discuss the overall variation of the computed lifetimes rather than analyzing their convergence, as shown below.

We find that the models with smaller NACs (e.g., after scaling them by smaller factors) show longer lifetimes and larger error bars, as expected. The lifetimes can vary by several hundred percent. The magnitude of such variations generally increases for slower dynamics (e.g., going down the rows in Figure 3), whereas it may be less sensitive to the details of the model Hamiltonian [e.g., comparing different models in each row (Figure 3)]. We further look into the influence of the number of frequencies on the lifetime convergence with respect to the repeated data unit length. As Figure 3 suggests, the presence of a larger number of frequencies in the NAC and energy gap data leads to faster dynamics in general (shorter lifetime) and to smaller variations of the computed lifetimes with respect to the repeated data unit length; the convergence is easier to reach. This observation can be rationalized as follows. The larger number of frequencies makes it more likely for the system to pass through points with larger NACs and smaller energy gaps. Indeed, we also observe that including more frequencies leads to larger fluctuations of NACs and energy gaps. The points with larger NACs and/or smaller energy gaps would be the main regions where the nonadiabatic transitions would often occur, contributing to the overall acceleration of the ground state recovery. Our calculations also suggest that in systems with strong electron−phonon coupling (and hence large NACs) and with a broad range of phonon modes, the repetition approach may be reasonably justified. The presence of many frequencies (especially the high-frequency ones) in the spectrum of a Hamiltonian means that a short repeated data unit used in the rNA-MD already samples the dominant frequencies and thus is an adequate sample of a longer trajectory. This also points to the important correlation between dispersion of the σ_X^2 parameter and lifetime convergence with respect to the original data length. In addition, the models with more frequencies generally show lifetimes shorter than those for the models with fewer frequencies in the spectrum of the Hamiltonian, i.e., model 7 versus model 3 in particular. We note that the contributions of the NAC and energy gap to the NA-MD are independent, as demonstrated with models 11 and 12, in which the frequencies of the NAC and energy gap FTs are swapped. The lifetime variation in model 12 is much smaller than that of model 11, leading us to conclude that the rNA-MD approach may be suitable for systems that contain a higher frequency of energy gaps and a low frequency of NACs.

To comprehensively characterize the variation of the lifetime across different regions of the parameter space, we consider the ratio of the lifetime computed for the vibronic Hamiltonian time series of a given length, t, τ_t, to the lifetime computed for the reference (100 ps) Hamiltonian data time series, $\tau_{100\ \mathrm{ps}}$. As shown in Figure 3, time scale τ_t can be larger or smaller than the reference time scale, $\tau_{100\ \mathrm{ps}}$. Because we are interested only in the magnitude of the variation of the time scales and not necessarily the "direction" (under- or overestimation), we consider both the ratio $\tau_t/\tau_{100\ \mathrm{ps}}$ and its inverse, $\tau_{100\ \mathrm{ps}}/\tau_t$.

https://doi.org/10.1021/acs.jpclett.2c02765
J. Phys. Chem. Lett. 2022, 13, 9688−9694

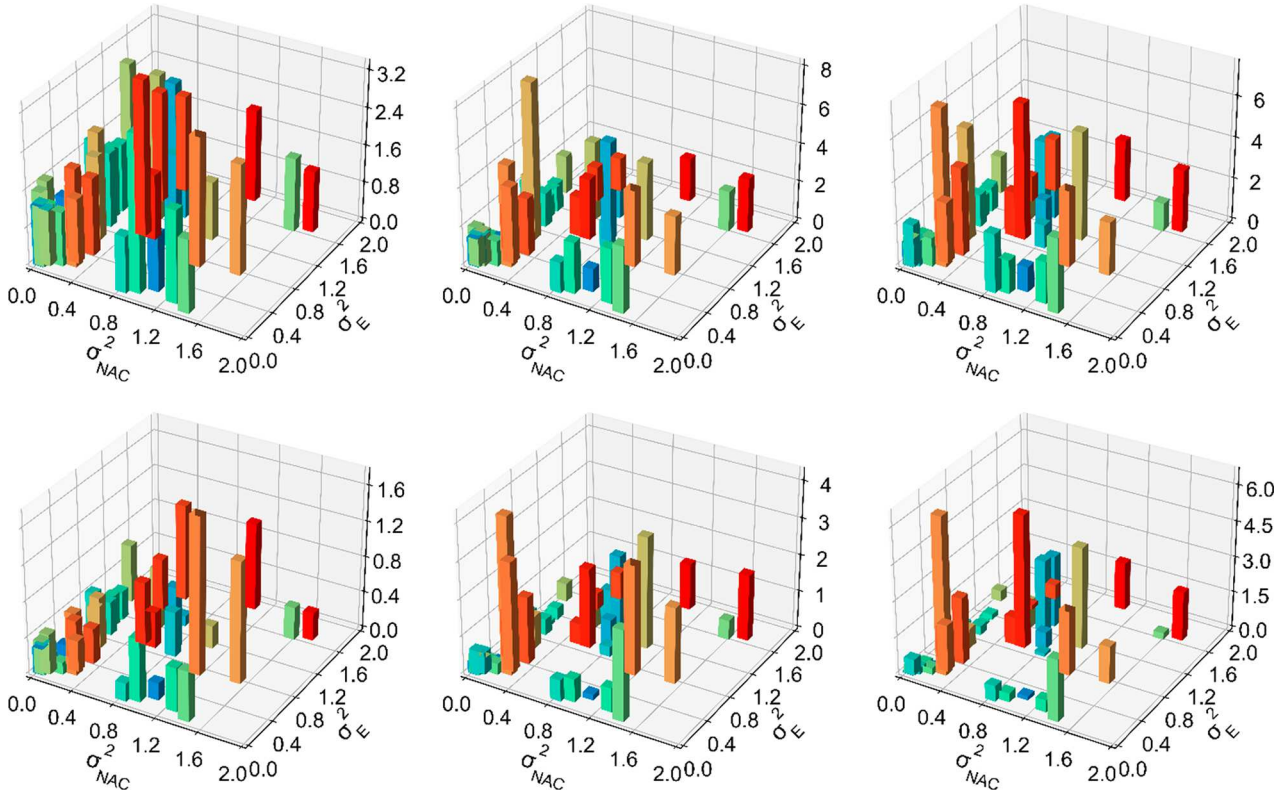

Figure 4. 3D representation of r^{max} (top row) and d^{max} (bottom row) in relation to σ_X^2 parameters for all two-state models. For columns 1−3, NAC scaled by 0.2, 0.1, and 0.05, respectively.

Considering various values of the repetition unit length, t, we compute the maximal ratio, r^{max}, and the maximal deviation, d^{max}:

$$r^{max} = \max_t \left(\frac{\tau_t}{\tau_{100\,ps}}, \frac{\tau_{100\,ps}}{\tau_t} \right) \tag{3a}$$

$$d^{max} = \max_t \left(\frac{|\tau_t - \tau_{100\,ps}|}{\tau_{100\,ps}} \right) \tag{3b}$$

The three-dimensional (3D) plots of r^{max} and d^{max} as functions of σ_X^2 (X is the energy gap or NAC) parameters for all of the considered models are shown in Figure 4, with the raw data listed in Tables S3 and S4. We recall that the large σ_X^2 corresponds to a large dispersion of frequencies present in the FT of the corresponding variable X. We hypothesize that larger values of σ_X^2 could lead to a larger dispersion of the time scales. However, we do not observe such a trend. Instead, the parameters r^{max} and d^{max} are distributed rather uniformly over a wide range of the σ_E^2 and σ_{NAC}^2 parameters, without a clear dependence. Nonetheless, we observe a clear trend in which both of these values increase when NACs are scaled down. This is consistent with our rationalization discussed above that the use of a small repetition data unit may be not representative of the entire trajectory, when the nonadiabatic couplings are weak. In this case, it is more probable to accidentally choose a subtrajectory with artificially faster or slower transitions. Hence, the possible variation of the computed time scales as a function of the repeated data unit may be large, whereas the convergence to the correct result may be slow.

We also characterize the magnitudes of the time scale variation as a function of the σ_X^2 parameters. For the NACs scaled by the factor of 0.2, for instance, we observe that r^{max} can reach 3.2, meaning that the computed time scales can be either 3.2 times smaller or 3.2 larger than the reference value obtained with the full set of 100 ps data. This ratio can reach 7−8 in the simulations with the original Hamiltonian NACs scaled down by factors of 0.05−0.1. Note that these deviations occur in a rather uncontrollable way depending on the length of the repeated date unit used. Using longer subtrajectories that are repeated does not necessarily guarantee the convergence to the reference value. In terms of the d^{max} parameter, the computed time scales may deviate by ≤120% (NAC scaling by a factor of 0.2) from the reference value all the way to >450% (NAC scaling by a factor of 0.05). Note that the d^{max} parameter does not directly translate the r^{max} parameter. For instance, a notable underestimation of the time scale with respect to the reference value may lead to small d^{max} magnitudes but large r^{max} values.

In summary, we have conducted a comprehensive assessment of the feasibility of the rNA-MD approach within the NBRA using a range of two-state model Hamiltonians. We find that the state transition time scales may strongly depend on the length of the repeated data, although the convergence is not monotonic and may be rather slow, making the repetition approach inaccurate. The computed time scales may be under- or overestimated compared to the reference values (derived from the explicit simulations without the variations) by a factor of ≤7−8. The overestimation or underestimation does not directly depend on the dispersion of frequencies in the spectra of energy gaps and NACs of the data; however, each depends on the magnitude of the NACs. The repetition approach

https://doi.org/10.1021/acs.jpclett.2c02765
J. Phys. Chem. Lett. 2022, 13, 9688−9694

becomes increasingly inaccurate in simulations with very small NACs, where the intrinsic transition are slow, on the order of ≥100 ps. Having said this, we understand that the repetition approach is not guaranteed to break down in individual simulations even in the case of intrinsically slow dynamics, but the errors, if they occur, may be more dramatic in this case. Although these results are given for simulations based on a simple FSSH scheme, we anticipate that more accurate schemes that account for decoherence effects may lead to even larger variations of computed lifetimes in response to the variation of the repeated unit length, because the inclusion of decoherence effects often slows the dynamics. In this regard, the presence of decoherence corrections in the dynamics may have an effect similar to decreasing the NACs, explored in this work. In addition, we observe that the presence of a larger number of frequencies in the FT of data (NACs and energy gaps) facilitate faster transitions. We expect that the results reported in this work can be used to assess the inaccuracies in applied rNA-MD simulations used by the practitioners and could serve as a general guide for using such a methodology.

■ ASSOCIATED CONTENT

Supporting Information

The Supporting Information is available free of charge at https://pubs.acs.org/doi/10.1021/acs.jpclett.2c02765.

Detailed parameters of model Hamiltonians, lifetime convergence plots for all models, and raw data of the maximal ratio and maximal deviation (PDF)

■ AUTHOR INFORMATION

Corresponding Author

Alexey V. Akimov − *Department of Chemistry, University at Buffalo, The State University of New York, Buffalo, New York 14260, United States;* orcid.org/0000-0002-7815-3731; Email: alexeyak@buffalo.edu

Author

Wei Li − *School of Chemistry and Materials Science, Hunan Agricultural University, Changsha 410128, China;* orcid.org/0000-0002-9999-5081

Complete contact information is available at: https://pubs.acs.org/10.1021/acs.jpclett.2c02765

Notes

The authors declare no competing financial interest.

■ ACKNOWLEDGMENTS

W.L. acknowledges financial support from the National Natural Science Foundation of China (21903023), the Science and Technology Innovation Program of Hunan Province (2021RC3089), and a Wallonie-Bruxelles International (WBI) Excellence scholarship. A.V.A. acknowledges financial support from the National Science Foundation (Grant NSF-2045204).

■ REFERENCES

(1) Akimov, A. V.; Neukirch, A. J.; Prezhdo, O. V. Theoretical Insights into Photoinduced Charge Transfer and Catalysis at Oxide Interfaces. *Chem. Rev.* **2013**, *113*, 4496−4565.

(2) Pal, S.; Trivedi, D. J.; Akimov, A. V.; Aradi, B.; Frauenheim, T.; Prezhdo, O. V. Nonadiabatic Molecular Dynamics for Thousand Atom Systems: A Tight-Binding Approach toward PYXAID. *J. Chem. Theory Comput.* **2016**, *12*, 1436−1448.

(3) Akimov, A. V. Nonadiabatic Molecular Dynamics with Tight-Binding Fragment Molecular Orbitals. *J. Chem. Theory Comput.* **2016**, *12*, 5719−5736.

(4) Hoff, D. A.; da Silva, R.; Rego, L. G. C. Coupled Electron−Hole Quantum Dynamics on D−π−A Dye-Sensitized TiO_2 Semiconductors. *J. Phys. Chem. C* **2012**, *116*, 21169−21178.

(5) da Silva, R.; Hoff, D. A.; Rego, L. G. C. Coupled Quantum-Classical Method for Long Range Charge Transfer: Relevance of the Nuclear Motion to the Quantum Electron Dynamics. *J. Phys.: Condens. Matter* **2015**, *27*, 134206.

(6) Shimojo, F.; Ohmura, S.; Mou, W.; Kalia, R. K.; Nakano, A.; Vashishta, P. Large Nonadiabatic Quantum Molecular Dynamics Simulations on Parallel Computers. *Comput. Phys. Commun.* **2013**, *184*, 1−8.

(7) Nebgen, B.; Prezhdo, O. V. Fragment Molecular Orbital Nonadiabatic Molecular Dynamics for Condensed Phase Systems. *J. Phys. Chem. A* **2016**, *120*, 7205−7212.

(8) Uratani, H.; Nakai, H. Non-Adiabatic Molecular Dynamics with Divide-and-Conquer Type Large-Scale Excited-State Calculations. *J. Chem. Phys.* **2020**, *152*, 224109.

(9) Carof, A.; Giannini, S.; Blumberger, J. Detailed Balance, Internal Consistency, and Energy Conservation in Fragment Orbital-Based Surface Hopping. *J. Chem. Phys.* **2017**, *147*, 214113.

(10) Uratani, H.; Yoshikawa, T.; Nakai, H. Trajectory Surface Hopping Approach to Condensed-Phase Nonradiative Relaxation Dynamics Using Divide-and-Conquer Spin-Flip Time-Dependent Density-Functional Tight Binding. *J. Chem. Theory Comput.* **2021**, *17*, 1290−1300.

(11) Wang, Z.; Dong, J.; Qiu, J.; Wang, L. All-Atom Nonadiabatic Dynamics Simulation of Hybrid Graphene Nanoribbons Based on Wannier Analysis and Machine Learning. *ACS Appl. Mater. Interfaces* **2022**, *14*, 22929−22940.

(12) Wang, B.; Chu, W.; Tkatchenko, A.; Prezhdo, O. V. Interpolating Nonadiabatic Molecular Dynamics Hamiltonian with Artificial Neural Networks. *J. Phys. Chem. Lett.* **2021**, *12*, 6070−6077.

(13) Akimov, A. V. Extending the Time Scales of Nonadiabatic Molecular Dynamics via Machine Learning in the Time Domain. *J. Phys. Chem. Lett.* **2021**, *12*, 12119−12128.

(14) Dral, P. O.; Barbatti, M.; Thiel, W. Nonadiabatic Excited-State Dynamics with Machine Learning. *J. Phys. Chem. Lett.* **2018**, *9*, 5660−5663.

(15) Chen, W.-K.; Liu, X.-Y.; Fang, W.-H.; Dral, P. O.; Cui, G. Deep Learning for Nonadiabatic Excited-State Dynamics. *J. Phys. Chem. Lett.* **2018**, *9*, 6702−6708.

(16) Hu, D.; Xie, Y.; Li, X.; Li, L.; Lan, Z. Inclusion of Machine Learning Kernel Ridge Regression Potential Energy Surfaces in On-the-Fly Nonadiabatic Molecular Dynamics Simulation. *J. Phys. Chem. Lett.* **2018**, *9*, 2725−2732.

(17) Li, X.; Xie, Y.; Hu, D.; Lan, Z. Analysis of the Geometrical Evolution in On-the-Fly Surface-Hopping Nonadiabatic Dynamics with Machine Learning Dimensionality Reduction Approaches: Classical Multidimensional Scaling and Isometric Feature Mapping. *J. Chem. Theory Comput.* **2017**, *13*, 4611−4623.

(18) Westermayr, J.; Gastegger, M.; Marquetand, P. Combining SchNet and SHARC: The SchNarc Machine Learning Approach for Excited-State Dynamics. *J. Phys. Chem. Lett.* **2020**, *11*, 3828−3834.

(19) Westermayr, J.; Gastegger, M.; Menger, M. F. S. J.; Mai, S.; González, L.; Marquetand, P. Machine Learning Enables Long Time Scale Molecular Photodynamics Simulations. *Chem. Sci.* **2019**, *10*, 8100−8107.

(20) Chen, W.-K.; Fang, W.-H.; Cui, G. Integrating Machine Learning with the Multilayer Energy-Based Fragment Method for Excited States of Large Systems. *J. Phys. Chem. Lett.* **2019**, *10*, 7836−7841.

(21) Akimov, A. V. Stochastic and Quasi-Stochastic Hamiltonians for Long-Time Nonadiabatic Molecular Dynamics. *J. Phys. Chem. Lett.* **2017**, *8*, 5190−5195.

(22) Wang, B.; Chu, W.; Prezhdo, O. V. Interpolating Nonadiabatic Molecular Dynamics Hamiltonian with Inverse Fast Fourier Transform. *J. Phys. Chem. Lett.* **2022**, *13*, 331−338.
(23) Li, L.; Long, R.; Prezhdo, O. V. Why Chemical Vapor Deposition Grown MoS_2 Samples Outperform Physical Vapor Deposition Samples: Time-Domain Ab Initio Analysis. *Nano Lett.* **2018**, *18*, 4008−4014.
(24) Li, L.; Long, R.; Bertolini, T.; Prezhdo, O. V. Sulfur Adatom and Vacancy Accelerate Charge Recombination in MoS_2 but by Different Mechanisms: Time-Domain Ab Initio Analysis. *Nano Lett.* **2017**, *17*, 7962−7967.
(25) Long, R.; Fang, W.; Prezhdo, O. V. Moderate Humidity Delays Electron−Hole Recombination in Hybrid Organic−Inorganic Perovskites: Time-Domain Ab Initio Simulations Rationalize Experiments. *J. Phys. Chem. Lett.* **2016**, *7*, 3215−3222.
(26) Liu, L.; Fang, W.-H.; Long, R.; Prezhdo, O. V. Lewis Base Passivation of Hybrid Halide Perovskites Slows Electron−Hole Recombination: Time-Domain Ab Initio Analysis. *J. Phys. Chem. Lett.* **2018**, *9*, 1164−1171.
(27) He, J.; Vasenko, A. S.; Long, R.; Prezhdo, O. V. Halide Composition Controls Electron−Hole Recombination in Cesium−Lead Halide Perovskite Quantum Dots: A Time Domain Ab Initio Study. *J. Phys. Chem. Lett.* **2018**, *9*, 1872−1879.
(28) Tully, J. C. Molecular Dynamics with Electronic Transitions. *J. Chem. Phys.* **1990**, *93*, 1061−1071.
(29) Craig, C. F.; Duncan, W. R.; Prezhdo, O. V. Trajectory Surface Hopping in the Time-Dependent Kohn-Sham Approach for Electron-Nuclear Dynamics. *Phys. Rev. Lett.* **2005**, *95*, 163001.
(30) Duncan, W. R.; Prezhdo, O. V. Theoretical Studies of Photoinduced Electron Transfer in Dye-Sensitized TiO_2. *Annu. Rev. Phys. Chem.* **2007**, *58*, 143−184.
(31) Akimov, A.; Libra, V. An Open-Source "Methodology Discovery" Library for Quantum and Classical Dynamics Simulations: SOFTWARE NEWS AND UPDATES. *J. Comput. Chem.* **2016**, *37*, 1626−1649.
(32) Akimov, A. V.; Shakiba, M.; Smith, B.; Sato, K.; Dutra, M.; Story, T.; Li, W.; Sun, X.; Stippell, L.; Chan, M.*Quantum-Dynamics-Hub/Libra-Code: Libra with the xTB/NA-MD Workflow*, ver. 5.2.0; Zenodo, 2022 (accessed 2022-10-06).
(33) Akimov, A. V.; Prezhdo, O. V. The PYXAID Program for Non-Adiabatic Molecular Dynamics in Condensed Matter Systems. *J. Chem. Theory Comput.* **2013**, *9*, 4959−4972.
(34) Li, W.; She, Y.; Vasenko, A. S.; Prezhdo, O. V. *Ab Initio* Nonadiabatic Molecular Dynamics of Charge Carriers in Metal Halide Perovskites. *Nanoscale* **2021**, *13*, 10239−10265.
(35) Chu, W.; Zheng, Q.; Prezhdo, O. V.; Zhao, J.; Saidi, W. A. Low-Frequency Lattice Phonons in Halide Perovskites Explain High Defect Tolerance toward Electron-Hole Recombination. *Sci. Adv.* **2020**, *6*, No. eaaw7453.
(36) Forde, A.; Kilin, D. Defect Tolerance Mechanism Revealed! Influence of Polaron Occupied Surface Trap States on CsPbBr3 Nanocrystal Photoluminescence: Ab Initio Excited-State Dynamics. *J. Chem. Theory Comput.* **2021**, *17*, 7224−7236.
(37) Li, L.; Long, R.; Bertolini, T.; Prezhdo, O. V. Sulfur Adatom and Vacancy Accelerate Charge Recombination in MoS_2 but by Different Mechanisms: Time-Domain Ab Initio Analysis. *Nano Lett.* **2017**, *17*, 7962−7967.
(38) Esteban-Puyuelo, R.; Sanyal, B. Role of Defects in Ultrafast Charge Recombination in Monolayer MoS_2. *Phys. Rev. B* **2021**, *103*, 235433.
(39) Long, R.; Fang, W.; Akimov, A. V. Nonradiative Electron−Hole Recombination Rate Is Greatly Reduced by Defects in Monolayer Black Phosphorus: Ab Initio Time Domain Study. *J. Phys. Chem. Lett.* **2016**, *7*, 653−659.
(40) Guo, Z.; Wang, J.; Yin, W.-J. Atomistic Origin of Lattice Softness and Its Impact on Structural and Carrier Dynamics in Three Dimensional Perovskites. *Energy Environ. Sci.* **2022**, *15*, 660−671.
(41) Hull, O. A.; Lingerfelt, D. B.; Li, X.; Aikens, C. M. Electronic Structure and Nonadiabatic Dynamics of Atomic Silver Nanowire−N2 Systems. *J. Phys. Chem. C* **2020**, *124*, 20834−20845.
(42) Trivedi, D. J.; Wang, L.; Prezhdo, O. V. Auger-Mediated Electron Relaxation Is Robust to Deep Hole Traps: Time-Domain Ab Initio Study of CdSe Quantum Dots. *Nano Lett.* **2015**, *15*, 2086−2091.
(43) Nelson, T. R.; Prezhdo, O. V. Extremely Long Nonradiative Relaxation of Photoexcited Graphane Is Greatly Accelerated by Oxidation: Time-Domain Ab Initio Study. *J. Am. Chem. Soc.* **2013**, *135*, 3702−3710.
(44) Li, W.; Long, R.; Hou, Z.; Tang, J.; Prezhdo, O. V. Influence of Encapsulated Water on Luminescence Energy, Line Width, and Lifetime of Carbon Nanotubes: Time Domain Ab Initio Analysis. *J. Phys. Chem. Lett.* **2018**, *9*, 4006−4013.
(45) Weight, B. M.; Sifain, A. E.; Gifford, B. J.; Kilin, D.; Kilina, S.; Tretiak, S. Coupling between Emissive Defects on Carbon Nanotubes: Modeling Insights. *J. Phys. Chem. Lett.* **2021**, *12*, 7846−7853.
(46) Zhou, G.; Cen, C.; Wang, S.; Deng, M.; Prezhdo, O. V. Electron−Phonon Scattering Is Much Weaker in Carbon Nanotubes than in Graphene Nanoribbons. *J. Phys. Chem. Lett.* **2019**, *10*, 7179−7187.
(47) Ren, J.; Vukmirović, N.; Wang, L.-W. Nonadiabatic Molecular Dynamics Simulation for Carrier Transport in a Pentathiophene Butyric Acid Monolayer. *Phys. Rev. B* **2013**, *87*, 205117.
(48) Li, W.*AkimovLab/Project_rNA-MD: Project_rNA-MD*, ver. 1.0.1; Zenodo, 2022 (accessed 2022-10-06).

https://doi.org/10.1021/acs.jpclett.2c02765
J. Phys. Chem. Lett. 2022, 13, 9688−9694